Published in final edited form as:
AJR Am J Roentgenol. 2010 October ; 195(4): 858–864. doi:10.2214/AJR.09.3766.

Time-Resolved and Bolus-Chase MR Angiography of the Leg: Branching Pattern Analysis and Identification of Septocutaneous Perforators

Gurpreet S. Sandhu[1,2], **Rod P. Rezaee**[3], **Katherine Wright**[2,4], **John A. Jesberger**[2], **Mark A. Griswold**[1,2,4], and **Vikas Gulani**[1,2]

[1]Department of Radiology, University Hospitals of Cleveland, Case Western Reserve University, 11100 Euclid Ave., Bolwell B 120, Cleveland, OH 44106

[2]Case Center for Imaging Research, Case Western Reserve University, Cleveland, OH

[3]Department of Otolaryngology–Head and Neck Surgery, University Hospitals of Cleveland, Case Western Reserve University, Cleveland, OH

[4]Department of Biomedical Engineering, University Hospitals of Cleveland, Case Western Reserve University, Cleveland, OH

Abstract

OBJECTIVE—The goal of this study was to compare time-resolved MR angiography (MRA) and bolus-chase MRA in the identification of peroneal artery septocutaneous perforators and for classification of the branching pattern of the arterial tree in the leg in a cohort of candidates for fibular free flap transfer operations.

MATERIALS AND METHODS—Retrospective analysis was performed on imaging data from 53 legs of 27 patients (age range, 27–88 years) who underwent time-resolved MRA (FLASH; TR/TE, 2.5/1.0; flip angle, 22°; voxel dimensions, 1.54 × 1.25 × 1.5 mm; acquisition time, 2.27 s/frame) and bolus-chase MRA (FLASH; 3.2/1.2; flip angle, 25°; voxel dimensions, 0.94 × 0.89 × 1 mm) at 3 T with gadobenate dimeglumine administered at 0.05 and 0.10 mmol/kg, respectively. The branching pattern was analyzed; the total number of septocutaneous perforators for each leg was calculated from the time-resolved and bolus-chase MRA data; and the results were combined. The total and average number of septocutaneous perforators per leg and the frequency of various branching patterns were calculated. The techniques were compared in terms of branching pattern and number of visible septocutaneous perforators.

RESULTS—A total of 84 septocutaneous perforators (1.58 ± 1.05 [SD] per leg) were identified. Pattern 1A was found in 42 legs; 1B, two legs; 2A, one leg; 2B, one; 3A, four; 3B, one; and 3D, two legs. Classification with time-resolved MRA was successful for 53 legs and with bolus-chase MRA for 51 legs ($Z = 0.713$, $p = 0.24$, one-tailed, not significant). Twenty-two septocutaneous perforators were identified with time-resolved MRA and 82 with bolus-chase MRA.

CONCLUSION—MRA of the leg can be used to investigate the branching pattern and identify septocutaneous perforators in a single step. With the imaging parameters and contrast dose used in this study, septocutaneous perforators can be better identified with bolus-chase MRA, although this result may be partially related to the higher gadolinium dose used in this technique.

Address correspondence to V. Gulani (vikas.gulani@uhhospitals.org)..

Keywords

fibula free-flap transfer operation; leg arterial tree branching pattern; MR angiography; septocutaneous perforator; time-resolved MR angiography

The fibular free flap transfer operation is a reconstructive procedure commonly performed after head and neck surgery. In this operation, a fibular free flap harvested from the leg is used for tissue reconstruction at the recipient site. A fibular free flap comprises a portion of the fibula, a fasciocutaneous component, and a part of the soleus or flexor hallucis longus muscle [1-3]. A peroneal artery septocutaneous perforator is desired in a fibular free flap to supply blood to the fasciocutaneous component of the flap [4]. The peroneal artery is dissected with the fibular free flap and is connected to a parent artery at the recipient site to minimize the risk of ischemic failure of the graft.

Accurate information about the branching pattern of the arterial tree in the leg is vital so that ischemic complications can be minimized at the recipient and donor sites after a fibular free flap transfer operation. A rudimentary or occluded peroneal artery cannot sustain blood supply to the fibular free flap tissue at the recipient site, the result being loss of the graft tissue. If, however, the peroneal artery is the sole or dominant source of blood to the foot, its excision can lead to foot ischemia [5].

Various imaging techniques such as CT angiography [6], MR angiography (MRA) [1], digital subtraction angiography [7], and color Doppler ultrasound [8] have been used for preoperative analysis of the branching pattern in candidates for fibular free flap transfer operations. The position of a peroneal artery septocutaneous perforator along the fibula determines the location of the harvest site and the size and shape of the fibular free flap [9]. Intraoperative ultrasound is commonly used to identify an appropriate septocutaneous perforator. Ultrasound, however, does not depict the entire course of a septocutaneous perforator or differentiate it from other types of perforators. Because it is performed during the operation, ultrasound imaging lengthens the dissection procedure. MRA has an edge over ultrasound in visualization of septocutaneous perforators because the inherent 3D capabilities of MRA enable visualization of the entire course of a septocutaneous perforator and help differentiate it from other types of perforators [1].

Candidates for fibular free flap transfer operations at our institution undergo hybrid MRA. The patients undergo stepping-table bolus-chase MRA and time-resolved MRA in the same session. In bolus-chase MRA, images are acquired at a number of stations from the abdomen to the legs, but venous contamination often impedes visualization of the arterial tree of the legs on these images [10]. In time-resolved MRA, a set of images are generated that can be used to obtain a snapshot of the arterial tree without venous contamination. Time-resolved image frames also can be used for accurate interpretation of the branching pattern in cases of arteriovenous fistula and stenotic lesions with retrograde flow in the arterial tree of the leg.

In this study, we analyzed the MRI data sets of a cohort of candidates for fibular free flap transfer operations to determine the frequency of the various branching patterns and to investigate individual variations in the frequency and location of peroneal artery septocutaneous perforators in the legs. We also compared time-resolved and bolus-chase MRA with respect to efficacy of branching pattern analysis and identification of septocutaneous perforators.

Materials and Methods

This study was HIPAA compliant and approved by the local institutional review board. From July 1, 2008, to April 1, 2009, 27 candidates for fibular free flap transfer operations (22 men, five women; mean age, 61.6 years; range, 27–88 years) underwent bolus-chase and time-resolved MRA examinations of the legs in the same session, and the images were retrospectively analyzed.

Image Acquisition

The MRI examinations were performed with a 3-T system (Magnetom Verio, Siemens Healthcare). Peripheral runoff and body coils were used for signal acquisition. The time-resolved imaging with stochastic trajectories technique was used for time-resolved MRA data acquisition. After a delay of 10 minutes, this procedure was followed by bolus-chase MRA of the legs as a part of abdominal angiography and peripheral runoff. The time-resolved and bolus-chase MRA examinations were performed with 0.05 and 0.10 mmol/kg of gadobenate dimeglumine (MultiHance, Bracco), respectively. During both examinations, the contrast agent was injected IV at a rate of 2 mL/s and followed by a saline flush (20 mL for each examination; rate, 2 mL/s).

Time-resolved angiography with interleaved stochastic trajectories is a 3D technique in which k-space undersampling is performed to accelerate the process of data acquisition. The whole k-space is sampled only once during data acquisition. At other times, data on all of a central 3D cylindrical region of the k-space (region A) are acquired for each image, whereas the peripheral region (region B) is undersampled. The missing data points in region B are filled by combining data from multiple frames. The proportion of region A with respect to the total k-space volume and the sampling fraction of region B in one frame are user specified [11].

Time-resolved angiography with interleaved stochastic trajectories data were acquired with a 3D T1-weighted FLASH sequence (TR/TE 2.5/1.0; flip angle, 22°; bandwidth, 1,115 Hz; field of view, 313 × 400 × 96 mm; matrix size, 203 × 320 × 64; generalized autocalibrating partially parallel acquisition factor, 2; partial-Fourier, 6/8; 25 images; temporal interpolation, 2; coronal reconstructions; frame rate, 4.54/s). The value of region A and percentage of data points of region B acquired during each frame were kept at 20% and 50%. These settings yielded time-resolved MRA images with voxel dimensions of 1.54 × 1.25 × 1.5 mm^3 at an average acquisition time of 2.27 s/frame. The bolus-chase MRA data were acquired with a 3D T1-weighted FLASH sequence (3.2/1.2; flip angle, 25°; bandwidth, 700 Hz; field of view, 350 × 400 × 96 mm^3; matrix size, 369 × 448 × 96; coronal sections). The voxel dimensions were 0.94 × 0.89 × 1 mm^3.

Image Analysis

Maximum intensity projection technique was used for data postprocessing and analysis. Both legs of all patients were evaluated (the one exception was a patient who had single leg). The bolus-chase and time-resolved MRA data on each leg were separately analyzed to estimate the total number and location of visible septocutaneous perforators and the branching pattern of the arterial tree of the leg. The information obtained from the two types of images was compared for individual legs and then combined. The information on septocutaneous perforators and branching pattern was used to identify ideal legs for flap harvest.

The source and the subtraction images were used to identify the septocutaneous perforators. Any branch of the peroneal artery that traversed the posterolateral intermuscular septum and reached the subcutaneous fascia without giving off a muscular branch was considered a

peroneal artery septocutaneous perforator [1, 2]. A few septocutaneous perforators identified with bolus-chase MRA were visible, partially visible, or not visible on time-resolved MRA images and vice versa.

A septocutaneous perforator was considered visible on an image only if the entire course from its origin to the fascial termination was identified. The number of visible septocutaneous perforators was separately calculated for each leg and each patient. The septocutaneous perforator visible on both types of images were counted only once. The numbers of visible septocutaneous perforators in all the legs were summed to obtain the total number of visible septocutaneous perforators. The average and distribution pattern of the number of visible septocutaneous perforators in individual legs and patients were separately analyzed. The vertical distance between the origin of each septocutaneous perforator and the inferior tip of the fibula also was measured.

The distribution pattern of septocutaneous perforators with respect to the distance of their origin from the lower end of fibula was studied. In its course through the intermuscular septum, a septocutaneous perforator can traverse a vertical distance down the leg before its fascial termination (vertical length). The vertical length of each septocutaneous perforator was measured, and the result was used to estimate the mean vertical length of all the septocutaneous perforators. The relation between the vertical length of the septocutaneous perforators and distance between their origin and the inferior tip of the fibula was analyzed with the Pearson correlation coefficient. The numbers of septocutaneous perforators originating along the proximal, middle, and distal thirds of the fibula and their respective mean vertical lengths were determined. The total numbers of septocutaneous perforators visible on bolus-chase and time-resolved MRA images and their distributions along the proximal, middle, and distal thirds of the fibula were calculated.

The subtraction data and subtraction maximum intensity projections were used to classify the branching patterns into the categories described in the literature [12]. The frequency of various branching patterns in the legs was analyzed. The total number of legs in which a type 3 anomaly was observed was determined. The total numbers of patients in whom a type 1 pattern was found in at least one leg and in whom the branching pattern was the same in both legs were separately calculated. The total number of legs in which the branching pattern classification was successfully identified on time-resolved and bolus-chase MRA images was separately analyzed. Whether the number of legs with successful classification with time-resolved MRA was statistically significantly greater than that with bolus-chase MRA was tested with a *Z* test of independent proportions at a significance level of $\alpha = 0.05$ (one tailed).

A candidate's ideal leg for fibular free flap harvest was defined as the one without moderate or severe stenosis in any of the anterior tibial, posterior tibial, and peroneal arteries and a minimum of one visible peroneal artery septocutaneous perforator. The total number of ideal candidate legs for fibular free flap harvest was determined. The total numbers of ideal candidate legs identified with time-resolved MRA and bolus-chase MRA were separately calculated. The significance of the difference between the number of ideal candidate legs identified with time-resolved MRA and with bolus-chase MRA was tested with a *Z* test of independent proportions (two-tailed, $\alpha = 0.05$).

Results

The total number of visible septocutaneous perforators was 84. The average number of visible septocutaneous perforators was 1.58 ± 1.05 (SD) per leg (range, 0–5) and 3.11 ± 1.80 per patient (range, 1–8). The distribution pattern of the number of septocutaneous

perforators with respect to the distance of their origin from the lower end of fibula is shown in Figure 1. The density of septocutaneous perforators was highest in the region 10–30 cm from the lower end of the fibula. There was a weak positive correlation (correlation coefficient, 0.39) between the vertical length of a septocutaneous perforator and the distance between its origin and the inferior tip of the fibula. The mean vertical length of the septocutaneous perforators was 2.23 ± 1.63 cm. The total number of septocutaneous perforators along each third of the fibula and their visibility on time-resolved and bolus-chase MRA images are shown in Table 1. The mean vertical lengths of the septocutaneous perforators with origins along the proximal, middle, and distal thirds of the fibula were 3.35 ± 2.42, 2.12 ± 1.38, and 1.72 ± 1.12 cm. A total of 82 septocutaneous perforators (97.6%) were visible with bolus-chase MRA and 22 septocutaneous perforators (26.2%) with time-resolved MRA.

The various branching patterns observed in this study are shown in Figure 2. The frequencies of the branching patterns are shown in Table 2. A type 3 anomaly was observed in seven legs (13.2%). A type 1 pattern was observed in at least one leg of 24 patients (88.9%). In 22 patients (81.5%), the branching pattern was the same for both the legs. Classification of the branching pattern was successful with time-resolved MRA in 53 legs and bolus-chase MRA in 51 legs ($Z = 0.713$, $p = 0.24$, one tailed, not significant). In the 51 legs in which the classification was successful with both time-resolved and bolus-chase MRA, the branching pattern types identified with the two techniques agreed. A total of 39 legs (73.6%) satisfied the ideal candidate leg criterion. The number of ideal candidate legs identified with bolus-chase MRA was 39 (73.6%) and with time-resolved MRA was 15 (28.3%) ($Z = 4.468$, $p < 0.01$, two-tailed, significant).

Discussion

MRA images constructed in virtually any plane can be used to visualize the full course of septocutaneous perforators and help differentiate them from other perforators (Fig. 3). At our institution, MRA findings on the legs of candidates for fibular free flap transfer operations previously were reported only in terms of the branching pattern and presence of any pathologic lesion in the arterial tree of the leg. The utility of MRA in the care of these patients can be further enhanced by reporting the number of septocutaneous perforators and their location with respect to a fixed point in the leg, which would aid planning of the location, size, and design of the graft.

The fibula is the longest bone in the human body available for autologous transplantation. Therefore, the leg is considered an optimal site for graft harvest in reconstructive surgery. However, some surgeons choose multiple flaps or an alternative flap, such as a scapular, iliac crest, or serratus anterior rib flap, to reconstruct complicated defects. Use of alternative or multiple flaps increases the flap harvest time, lengthens recovery time, increases exposure to serious complications, and increases overall morbidity compared with that associated with a fibular free flap. Preoperative analysis may allow the surgeon to know whether to use a fibular free flap for more complicated defects. A priori characterization of septocutaneous perforators would give the surgeon confidence that the vascularity of a larger than standard cutaneous skin paddle could be supported and harvested for the reconstruction.

A pilot study [9] showed the successful use of MRA in branching pattern analysis and visualization of septocutaneous perforators at the same time in candidates for fibular free flap transfer operations. Our study involved a relatively large number of legs, and we compared two MRA techniques at the same time. Inclusion of a larger number of legs enabled us to compare the visibility of septocutaneous perforators on MRA images with the findings at cadaver dissection [2, 13-16]. The frequency of the visible septocutaneous

perforators in one leg in our study matched that in previous reports [14-16]. However, the number of legs without a septocutaneous perforator is relatively high [2, 14-16], probably because of the low spatial resolution of MRA compared with the diameters of septocutaneous perforators. The average diameter of a peroneal artery septocutaneous perforator at the origin is 1.2 ± 0.4 mm and at the fascial termination is 0.6 ± 0.2 mm [13].

That most of the septocutaneous perforators (82.2%) were located along the distal two thirds of the fibula (Table 2) is also in agreement with previous reports [1, 2, 13, 17]. We analyzed the distribution pattern of the septocutaneous perforators with the inferior tip of the fibula as a reference because it was visible in the field of view of all of the images. The head of the fibula can also be used as the reference for location of septocutaneous perforators [1]. The number of septocutaneous perforators visible with bolus-chase MRA was 3.8 times higher than that with time-resolved MRA. The contrast between the septocutaneous perforators and adjacent structures was lower with time-resolved than with bolus-chase MRA (Fig. 3). The low visibility of septocutaneous perforators on time-resolved MRA images in this study likely relates to lower spatial resolution and lower gadolinium dose used in this technique. We used a half dose of gadolinium for time-resolved MRA examinations to keep the total contrast dose for individual patients to a minimum, and the clinical protocol was not designed with a research study in mind. Use of a full gadolinium dose would improve the visibility of small vessels such as septocutaneous perforators. The spatial resolution of time-resolved MRA also conceivably can be improved by sacrificing temporal resolution.

A number of studies have shown the frequency of various branching patterns in the arterial tree of the leg [6, 12, 18, 19]. Type 1 is the most common branching pattern, but anatomic variations in 7.8–12% of legs have been reported. The branching patterns can also vary between the two legs of an individual. When the branching pattern is anomalous in one leg, the probability is higher (28%) that the other leg also has an anomalous branching pattern [19]. Type 3 anomalies are particularly prone to ischemic complications after a fibular free flap transfer operation. Flap harvest from a leg with a subtype 3C (peronea arteria magna) anomaly is associated with particularly high risk of foot ischemia. A subtype 3D anomaly, however, increases the difficulty of establishing a blood supply to the fibular free flap at the recipient site. The frequency of type 3 anomaly was relatively high in our study compared with previously reported findings [18, 19]. The difference between time-resolved and bolus-chase MRA for successful classification of the branching pattern was not statistically significant. In the cases of two patients, bolus-chase MRA from subtraction data and from maximum intensity projections did not depict the branching pattern in one leg owing to the presence of excessive collateral circulation and venous contamination. Venous contamination is a particular problem with bolus-chase MRA in cases in which contrast bolus movement differs between the two legs of a patient. In those cases, acquisition of time-resolved MRA frames at different times can be used for analysis of the branching pattern (Fig. 4).

The number of ideal candidate legs identified with bolus-chase MRA was significantly greater than that identified with time-resolved MRA, primarily because of the higher visibility of septocutaneous perforators with the former technique. Fourteen legs (26.4%) in 10 patients (37.0%) did not satisfy the ideal candidate leg criterion. MRA would have played a role in localization of the fibular free flap harvest site in these patients. No septocutaneous perforator was visible in three legs (5.7%). In these legs, the fibular free flap can be centered on a septomusculocutaneous perforator, but this technique complicates the dissection process. Branching pattern abnormalities and stenotic lesions were found in 12 legs (22.6%) (in one of the legs, in addition to peroneal artery occlusion, no septocutaneous perforator was identified). Harvest of a fibular free flap from these limbs carries higher risk of ischemic complications. Even in ideal candidate legs, preoperative imaging plays a role in

surgical decision making by helping in location of the harvest site and design of a fibular free flap. Previous studies [5-7, 20-24] have shown that preoperative imaging influences the surgical approach in the care of as many as 55.2% [24] of patients.

A number of techniques have been described for preoperative evaluation of candidates for fibular free flap transfer operations. History and physical examination are considered important aspects of the evaluation [25]. Examination of pedal pulses [25] and the ankle–arm index [26, 27] can be reliably used to detect occlusive lesions. However, the presence of congenital vascular variations necessitates preoperative imaging [27]. Digital subtraction angiography has been considered the reference standard for preoperative analysis in the care of these patients [7], but this invasive procedure yields only 2D images, does not depict septocutaneous perforators, entails exposure to ionizing radiation, and is associated with a small but definite rate of complications [1, 5, 28]. Color Doppler ultrasound is a noninvasive imaging technique without ionizing radiation exposure, but its operator dependency and lack of depiction of branching patterns and the entire course of perforators and differentiation of perforator types are its main limitations [1, 28].

CT angiography and MRA are noninvasive techniques and yield 3D images in any arbitrary plane. They provide accurate information regarding branching pattern and can be used to identify septocutaneous perforators [1, 28]. CT angiograms can be obtained with high spatial resolution (0.3 mm), but a CT examination exposes patients to ionizing radiation [28]. MRA, however, generates images with high spatial resolution, does not expose the patient to ionizing radiation, and can be performed in multiple phases without posing additional risk or harm to the patient [1, 28]. An additional advantage of bolus-chase MRA is that images from proximal stations can be used to analyze the vascular anatomy of the abdominal aorta and other large arteries; occlusive lesions in proximal blood vessels are considered contraindications to fibular free flap harvest [29]. The visibility of septocutaneous perforators is poor with time-resolved MRA performed with the imaging parameters and gadolinium contrast dose used in this study. There also was no significant difference between time-resolved and bolus-chase MRA with respect to visualization of branching patterns.

A weakness of our study was that the bolus-chase MRA examination was performed after the time-resolved examination, and venous contamination on the bolus-chase MRA images might have been related to the gadolinium contrast injection for time-resolved MRA. However, we allowed a 10-minute interval after the initial injection to minimize this problem, and venous contamination from the first study was found not to be a factor. The use of subtraction images eliminated this effect. Other weaknesses were that there was no reference standard examination in this study and that the location of the septocutaneous perforators was not confirmed prospectively. This issue can be addressed in a future study. To further validate the use of MRA for fibular free flap transfer operations, the optimum harvest site identified with MRA can be compared with the actual harvest site used for the operation. The visibility of septocutaneous perforators with MRA can be further improved by increasing the spatial resolution to a submillimeter level and optimizing the gadolinium contrast dose.

MRA of the legs can be used to analyze the branching pattern of the lower leg arterial tree and to identify peroneal artery septocutaneous perforators in a single step. The addition of time-resolved MRA with the imaging parameters and gadolinium contrast dose used in this study does not offer substantial advantage over bolus-chase MRA alone. Further work with a higher contrast dose and improved spatial resolution is needed.

Acknowledgments

Supported by Siemens Healthcare (G. S. Sandhu and M. A. Griswold) and NIH/NCRR grant 1KL2RR024990 (V. Gulani).

References

1. Fukaya E, Grossman RF, Saloner D, Leon P, Nozaki M, Mathes SJ. Magnetic resonance angiography for free fibula flap transfer. J Reconstr Microsurg. 2007; 23:205–211. [PubMed: 17530612]
2. Schusterman MA, Reece GP, Miller MJ, Harris S. The osteocutaneous free fibula flap: is the skin paddle reliable? Plast Reconstr Surg. 1992; 90:787–793. discussion 794-798. [PubMed: 1410031]
3. Chen ZW, Yan W. The study and clinical application of the osteocutaneous flap of fibula. Microsurgery. 1983; 4:11–16. [PubMed: 6633239]
4. Futran ND, Stack BC Jr, Payne LP. Use of color Doppler flow imaging for preoperative assessment in fibular osteoseptocutaneous free tissue transfer. Otolaryngol Head Neck Surg. 1997; 117:660–663. [PubMed: 9419095]
5. Young DM, Trabulsy PP, Anthony JP. The need for preoperative leg angiography in fibula free flaps. J Reconstr Microsurg. 1994; 10:283–287. discussion 287-289. [PubMed: 7996510]
6. Chow LC, Napoli A, Klein MB, Chang J, Rubin GD. Vascular mapping of the leg with multi-detector row CT angiography prior to free-flap transplantation. Radiology. 2005; 237:353–360. [PubMed: 16100083]
7. Seres L, Csaszar J, Voros E, Borbely L. Donor site angiography before mandibular reconstruction with fibula free flap. J Craniofac Surg. 2001; 12:608–613. [PubMed: 11711831]
8. Futran ND, Stack BC Jr, Zaccardi MJ. Preoperative color flow Doppler imaging for fibula free tissue transfers. Ann Vasc Surg. 1998; 12:445–450. [PubMed: 9732422]
9. Fukaya E, Saloner D, Leon P, Wintermark M, Grossman RF, Nozaki M. Magnetic resonance angiography to evaluate septocutaneous perforators in free fibula flap transfer. J Plast Reconstr Aesthet Surg. 2010; 63:1099–1104. [PubMed: 19577973]
10. Wang Y, Winchester PA, Khilnani NM, et al. Contrast-enhanced peripheral MR angiography from the abdominal aorta to the pedal arteries: combined dynamic two-dimensional and bolus-chase three-dimensional acquisitions. Invest Radiol. 2001; 36:170–177. [PubMed: 11228581]
11. Song T, Laine AF, Chen Q, et al. Optimal k-space sampling for dynamic contrast-enhanced MRI with an application to MR renography. Magn Reson Med. 2009; 61:1242–1248. [PubMed: 19230014]
12. Bardsley JL, Staple TW. Variations in branching of the popliteal artery. Radiology. 1970; 94:581–587. [PubMed: 5413899]
13. Yoshimura M, Shimada T, Hosokawa M. The vasculature of the peroneal tissue transfer. Plast Reconstr Surg. 1990; 85:917–921. [PubMed: 2349296]
14. Jones NF, Monstrey S, Gambier BA. Reliability of the fibular osteocutaneous flap for mandibular reconstruction: anatomical and surgical confirmation. Plast Reconstr Surg. 1996; 97:707–716. discussion 717-708. [PubMed: 8628764]
15. Wei FC, Chen HC, Chuang CC, Noordhoff MS. Fibular osteoseptocutaneous flap: anatomic study and clinical application. Plast Reconstr Surg. 1986; 78:191–200. [PubMed: 3523559]
16. Beppu M, Hanel DP, Johnston GH, Carmo JM, Tsai TM. The osteocutaneous fibula flap: an anatomic study. J Reconstr Microsurg. 1992; 8:215–223. [PubMed: 1629801]
17. Winters HA, de Jongh GJ. Reliability of the proximal skin paddle of the osteocutaneous free fibula flap: a prospective clinical study. Plast Reconstr Surg. 1999; 103:846–849. [PubMed: 10077073]
18. Kim D, Orron DE, Skillman JJ. Surgical significance of popliteal arterial variants: a unified angiographic classification. Ann Surg. 1989; 210:776–781. [PubMed: 2589890]
19. Kil SW, Jung GS. Anatomical variations of the popliteal artery and its tibial branches: analysis in 1242 extremities. Cardiovasc Intervent Radiol. 2009; 32:233–240. [PubMed: 18982387]
20. Blackwell KE. Donor site evaluation for fibula free flap transfer. Am J Otolaryngol. 1998; 19:89–95. [PubMed: 9550438]

21. Kessler P, Wiltfang J, Schultze-Mosgau S, Lethaus B, Greess H, Neukam FW. The role of angiography in the lower extremity using free vascularized fibular transplants for mandibular reconstruction. J Craniomaxillofac Surg. 2001; 29:332–336. [PubMed: 11777350]
22. Carroll WR, Esclamado R. Preoperative vascular imaging for the fibular osteocutaneous flap. Arch Otolaryngol Head Neck Surg. 1996; 122:708–712. [PubMed: 8663940]
23. Lorenz RR, Esclamado R. Preoperative magnetic resonance angiography in fibular-free flap reconstruction of head and neck defects. Head Neck. 2001; 23:844–850. [PubMed: 11592231]
24. Lohan DG, Tomasian A, Krishnam M, Jonnala P, Blackwell KE, Finn JP. MR angiography of lower extremities at 3 T: presurgical planning of fibular free flap transfer for facial reconstruction. AJR. 2008; 190:770–776. [PubMed: 18287451]
25. Clemenza JW, Rogers S, Magennis P. Pre-operative evaluation of the lower extremity prior to microvascular free fibula flap harvest. Ann R Coll Surg Engl. 2000; 82:122–127. [PubMed: 10743434]
26. Futran ND, Stack BC Jr, Zachariah AP. Ankle-arm index as a screening examination for fibula free tissue transfer. Ann Otol Rhinol Laryngol. 1999; 108:777–780. [PubMed: 10453786]
27. Klein S, Hage JJ, van der Horst CM, Lagerweij M. Ankle-arm index versus angiography for the pre-assessment of the fibula free flap. Plast Reconstr Surg. 2003; 111:735–743. [PubMed: 12560694]
28. Rozen WM, Ashton MW, Stella DL, Phillips TJ, Taylor GI. Magnetic resonance angiography and computed tomographic angiography for free fibular flap transfer. J Reconstr Microsurg. 2008; 24:457–458. [PubMed: 18668474]
29. Kelly AM, Cronin P, Hussain HK, Londy FJ, Chepeha DB, Carlos RC. Preoperative MR angiography in free fibula flap transfer for head and neck cancer: clinical application and influence on surgical decision making. AJR. 2007; 188:268–274. [PubMed: 17179376]

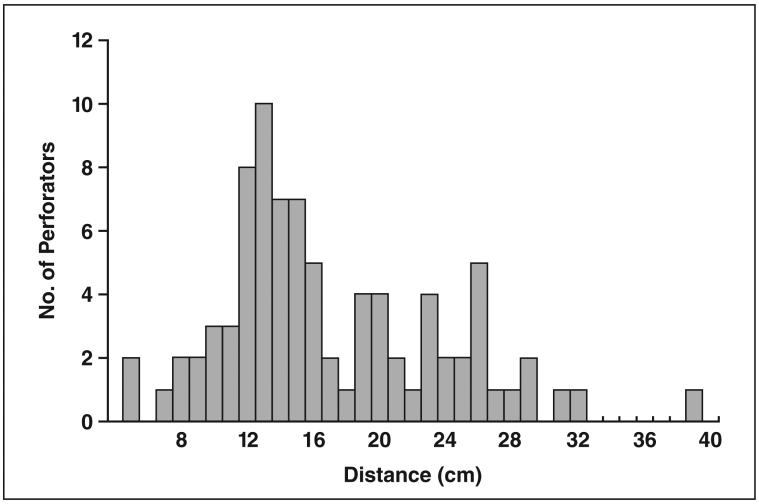

Fig. 1.
The number of peroneal artery septocutaneous perforators as function of distance between origin and lower end of fibula.

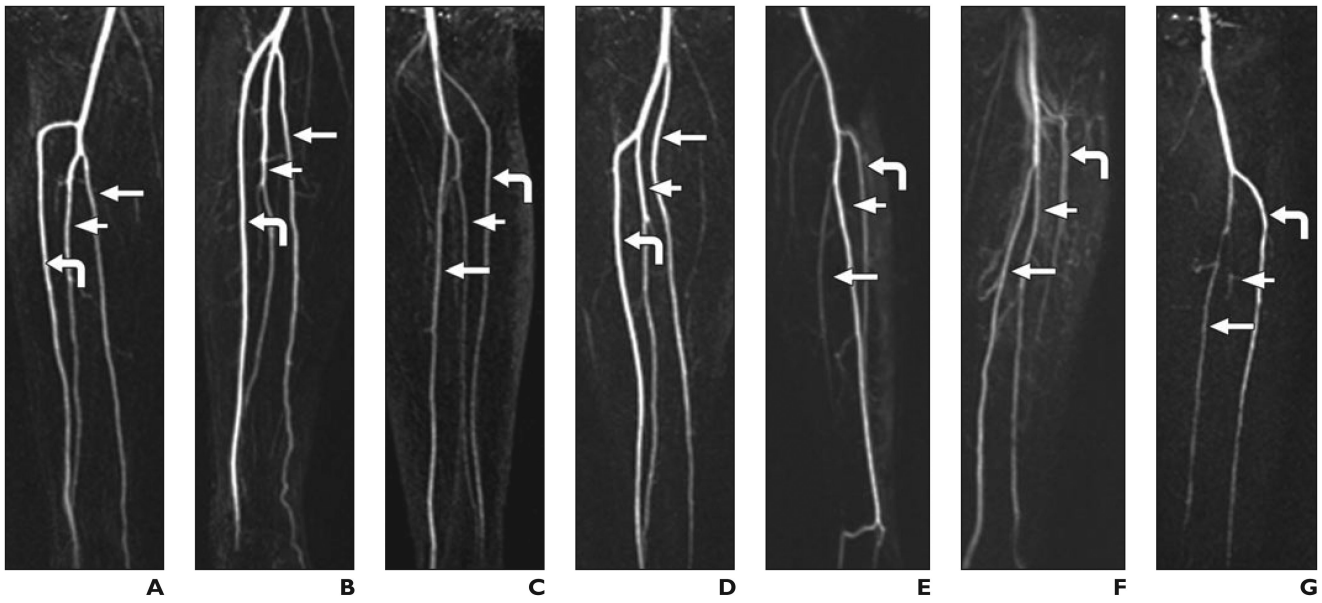

Fig. 2.

Full-thickness maximum intensity projections of subtraction data from time-resolved MR angiography show various branching patterns observed in study. Curved arrow indicates anterior tibial artery; long straight arrow, posterior tibial artery; short straight arrow, peroneal artery.

A, Pattern 1A. Anterior tibial artery originates below knee, below which is bifurcation of tibioperoneal trunk into posterior tibial artery and peroneal artery.

B, Pattern 1B. Anterior tibial artery, posterior tibial artery, and peroneal artery originate below knee within 0.5 cm of one another.

C, Pattern 2A. Anterior tibial artery originates at or above knee joint.

D, Pattern 2B. Posterior tibial artery originates at knee, and common trunk of anterior tibial artery and peroneal artery is present.

E, Pattern 3A. Anterior tibial artery is normal, posterior tibial artery is hypoplastic, and plantar arteries in foot are supplied by peroneal artery.

F, Pattern 3B. Hypoplastic or aplastic anterior tibial artery is distally replaced by peroneal artery, and dorsalis pedis artery is replaced by peroneal artery.

G, Pattern 3D. Hypoplastic or aplastic peroneal artery.

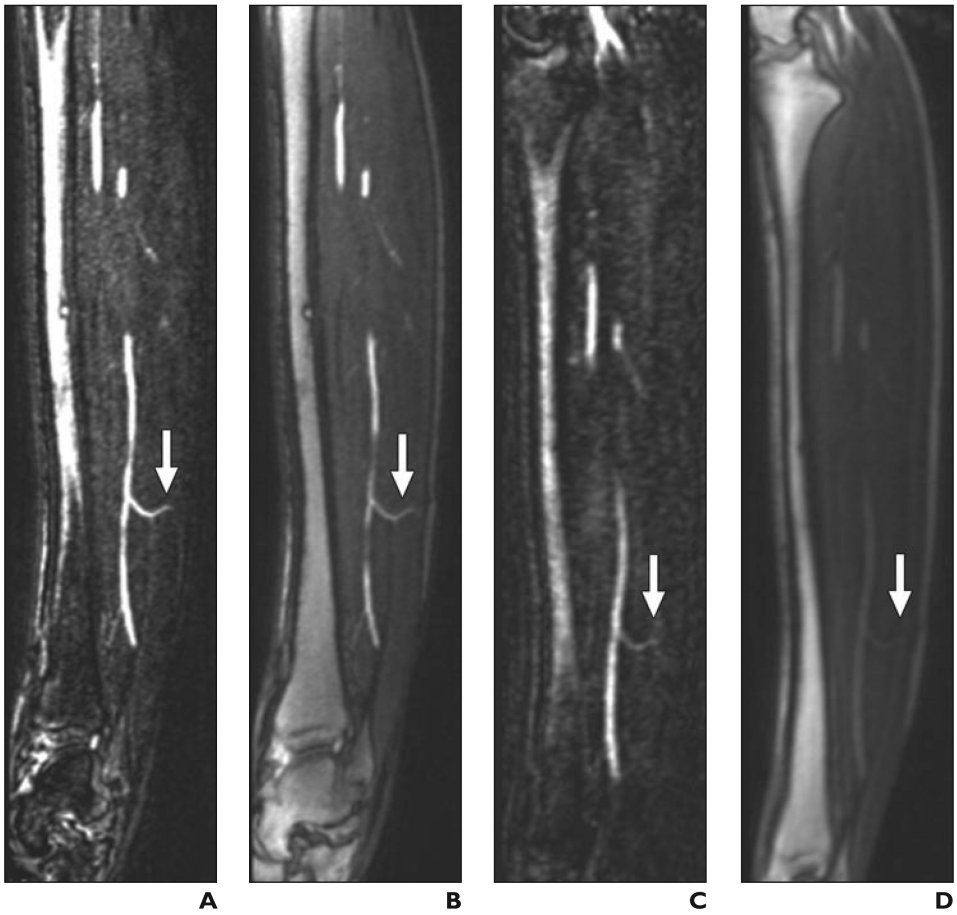

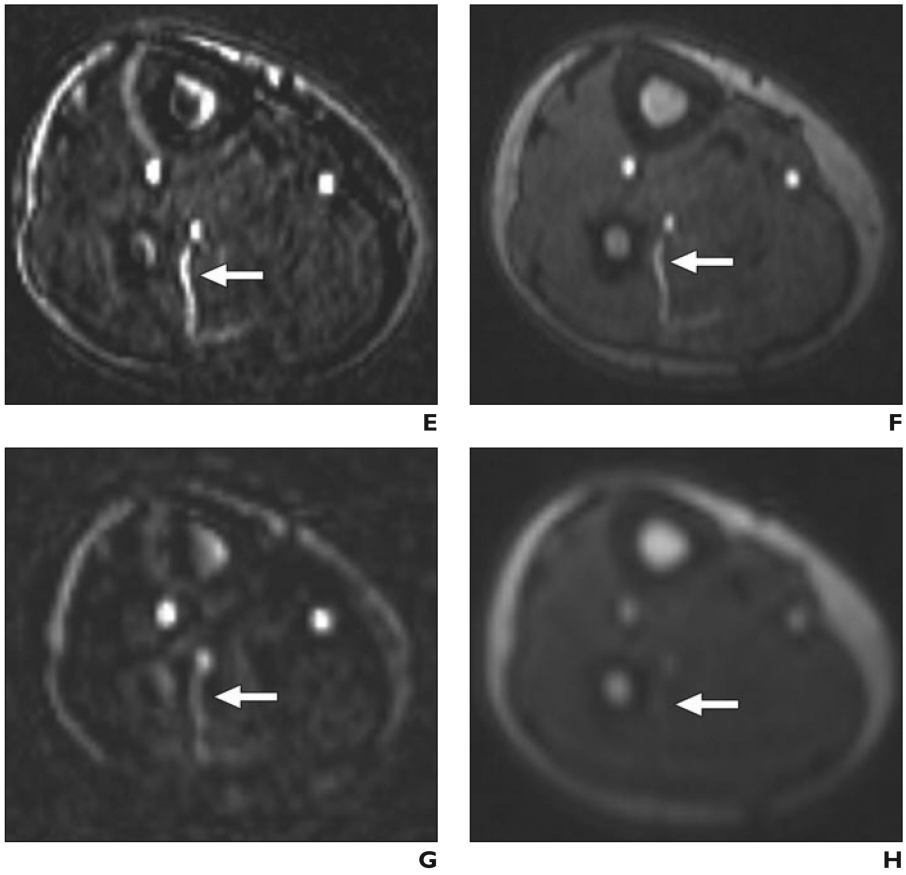

Fig. 3.
Septocutaneous perforator.
A–H, Sagittal (**A–D**) and axial (**E–H**) maximum-intensity-projection (MIP) (3 mm thick) images show septocutaneous perforator (*arrow*) on sagittal MIPs from subtraction and source data from bolus-chase MR angiograms (**A** and **B,** respectively) and time-resolved MR angiograms (**C** and **D**). Same septocutaneous perforator is evident on axial MIPs from subtraction and source data from bolus-chase MR angiogram (**E** and **F**) and time-resolved MR angiograms (**G** and **H**). Structures surrounding perforator can be identified on source images, which help in location of path of septocutaneous perforator. Contrast between septocutaneous perforator and surrounding soft tissues is relatively low on unsubtracted time-resolved MR angiograms. **A–H**, Sagittal (**A–D**) and axial (**E–H**) maximum-intensity-projection (MIP) (3 mm thick) images show septocutaneous perforator (*arrow*) on sagittal MIPs from subtraction and source data from bolus-chase MR angiograms (**A** and **B,** respectively) and time-resolved MR angiograms (**C** and **D**). Same septocutaneous perforator is evident on axial MIPs from subtraction and source data from bolus-chase MR angiogram (**E** and **F**) and time-resolved MR angiograms (**G** and **H**). Structures surrounding perforator can be identified on source images, which help in location of path of septocutaneous perforator. Contrast between septocutaneous perforator and surrounding soft tissues is relatively low on unsubtracted time-resolved MR angiograms.

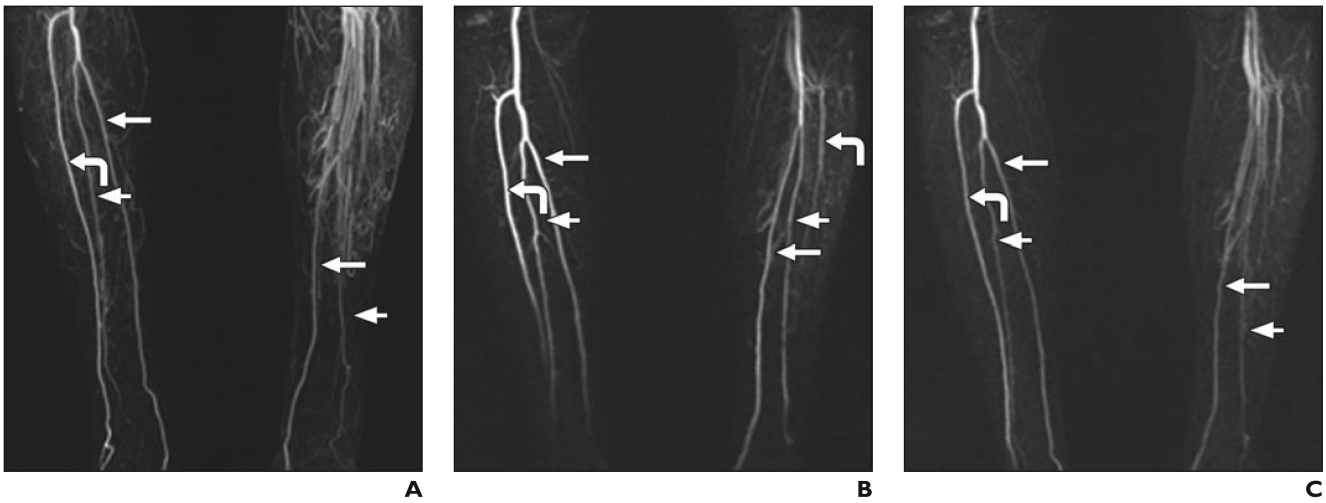

Fig. 4.

Patient in whom branching pattern of left leg could not be classified with bolus-chase MR angiography.

A–C, Bolus-chase (**A**) and time-resolved (**B** and **C**) MR angiograms. Branching pattern was classified as type 3A on time-resolved MR angiograms. Branching patterns of left (**B**) and right (**C**) legs is best delineated on two time-resolved MR angiograms images obtained 15 seconds apart. Curved arrow indicates anterior tibial artery; long straight arrow, posterior tibial artery; short arrow, peroneal artery. Anterior tibial and peroneal arteries is not evident in **A**, and anterior tibial artery is not evident in **C.**

TABLE 1
Visibility of Septocutaneous Perforators on MR Angiograms

Fibular Region	Total No. of Septocutaneous Perforators	Time-Resolved		Bolus-Chase	
		Visible	Not or Partially Visible	Visible	Not or Partially Visible
Proximal third	15 (17.9)	3	12	15	0
Middle third	47 (56.0)	13	34	46	1
Distal third	22 (26.2)	6	16	21	1
Total	84 (100)	22	62	82	2

Note—Values are number of perforators; values in parentheses are percentages.

TABLE 2

Frequency of Branching Patterns in Lower Leg Arterial Tree Identified With MR Angiography

Branching Pattern	Frequency	
	Bolus-Chase	Time-Resolved
1A	42 (79.2)	42 (79.2)
1B	2 (3.8)	2 (3.8)
2A	1 (1.9)	1 (1.9)
2B	1 (1.9)	1 (1.9)
3A	3 (5.7)	4 (7.5)
3B	0 (0)	1 (1.9)
3D	2 (3.8)	2 (3.8)
Not identified	2 (3.8)	0 (0)
Total	53 (100)	53 (100)

Note—Values are number of perforators; values in parentheses are percentages.